Simplified High-Accuracy Calculation of Eddy-Current Losses in Round-Wire Windings

Xi Nan
C. R. Sullivan

Simplified High-Accuracy Calculation of Eddy-Current Loss in Round-Wire Windings

Xi Nan
Thayer School of Engineering
Dartmouth College, USA
Email: xi.nan@dartmouth.edu

Charles R. Sullivan
Thayer School of Engineering
Dartmouth College, USA
Email: Charles.R.Sullivan@dartmouth.edu

Abstract— **It has recently been shown that the most commonly used methods for calculating high-frequency eddy-current loss in round-wire windings can have substantial error, exceeding 60%. Previous work includes a formula based on a parametric set of finite-element analysis (FEA) simulations that gives proximity-effect loss for a large range of frequencies, using the parameters from a lookup table based on winding geometry. We improve the formula by decreasing the number of parameters in the formula and also, more importantly, by using simple functions to get the parameters from winding geometry such that a large lookup table is not needed. The function we present is exact in the low frequency limit (diameter much smaller than skin depth) and has error less than 4% at higher frequencies.**

We make our new model complete by examining the field expression needed to get the total proximity-effect loss and by including the skin-effect loss. We also present experimental results confirming the validity of the model and its superiority to standard methods.

I. INTRODUCTION

In the design and optimization of magnetic components such as inductors and transformers used in power electronics applications, accurate prediction of high-frequency winding loss is very important. Eddy-current winding loss, which includes skin-effect loss and proximity-effect loss, increases rapidly with frequency. Due to the complexity of winding geometries and interactions between conductors in windings, it is difficult to find a general analytical solution for the eddy-current losses in windings. Several methods have been used to predict high-frequency winding losses in windings of round conductors as reviewed in [1]. One type of these methods [2], [3], [4], [5], [6], often called the Dowell method, is to use the analytical solution for a foil conductor as an equivalent to round conductors in the same layer with the same total cross-sectional area. Another type of method is called the Ferreira method or the Bessel-function method [7], [8], [9], [10], [11], which is to use the analytical field solution of a single isolated round conductor which is subjected to an external uniform field.

Both the Dowell method and the Bessel-function method can have large error (up to 60% to 150%) at high frequencies [12]. Another kind of approach used to calculate eddy-current loss is to employ numerical methods such as finite element analysis (FEA) to find the field solutions. Through FEA, it is possible to find the loss for any given configuration to any desired degree of accuracy, though it may be very time-consuming and one solution can only be applied to one certain configuration. Several approaches [13], [14] have been used to overcome the limitations of direct numerical methods as discussed in [12].
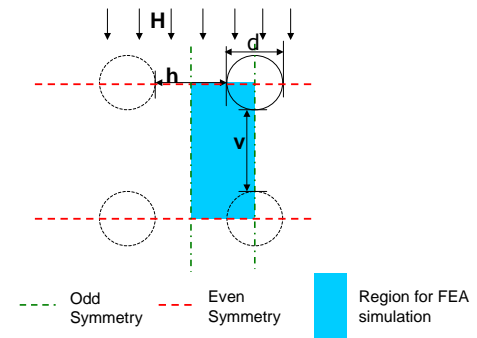
Fig. 1. FEA simulation configuration for a rectangular winding of round conductors. The power loss in the shaded area represents half the proximity-effect loss per unit length in each turn of a winding with interwire distance v and interlayer distance h.

To find the behavior of a round wire in a winding, [12] used FEA for a single wire with symmetry boundary conditions as shown in Fig. 1. Loss in the simulation region can represent proximity-effect loss in half of a round conductor in a winding with interlayer distance h and interwire distance v. The setup of the boundary conditions was discussed in detail in [12]. Reference [12] collected data of power loss and field solutions for a range of wire spacings in two directions and for ratios of wire diameter to skin depth ranging from 0.6 to 60, and showed that the proximity-effect loss factor, which is proximity-effect loss in a conductor normalized by the square of the external field, not only increases with frequency, but also depends on the interwire distance in a layer and the interlayer distance. Based on these results, [12] gives a function that approximates the simulation results much better (error less than 2%), and provides a table in which the parameters of the function can be looked up according to the wire spacings.

In this paper, we improve on the model provided in [12]. As in [12], the new model gives a more accurate loss prediction than the Dowell method or the Bessel-function method, and works for a large range of frequencies and for any wire size and winding geometry used in practice. However, the functions have been simplified and adjusted to give exact results matching analytical solutions in the low-frequency limit, and the new model does not require a large table of parameters as in [12], but instead uses simple functions to get the parameters from winding geometry. In addition to presenting this improved model for proximity-effect loss factor, we examine the field expression needed to get the total proximity-effect loss, discuss

the inclusion of the skin-effect loss, and show that using a simple model for skin-effect loss gives only small errors. Thus, we are able to provide a complete model for calculating the winding losses for round conductors configured as shown in Fig. 1. We also present experimental results confirming the validity of the model and its superiority to standard methods.

Section II discusses in detail how we decompose eddy-current loss into skin-effect loss and proximity-effect loss. In Section III, the model for calculating proximity-effect loss factor is presented and its accuracy is analyzed. Section IV shows how to calculate the total 'proximity field' in a winding, which is another important factor that determines the total proximity-effect loss besides proximity-effect loss factor. In Section V, we discuss the calculation of skin-effect loss. Experimental results are given in Section VI that prove the validity of our model.

II. DEFINITIONS AND DECOMPOSITION OF SKIN-EFFECT LOSS AND PROXIMITY-EFFECT LOSS

Winding loss at high frequencies is caused by eddy-current effects. Generally, eddy-current effects are divided into skin effect and proximity effect. The classical definition of skin-effect loss is the extra AC loss in a single isolated conductor which is carrying a time-varying current. And the corresponding definition of proximity-effect loss in a winding is defined as the total eddy-current loss minus the classical skin-effect loss.

The classical definitions of skin-effect loss and proximity-effect loss can help us better understand the behavior of a conductor at high frequencies. However, they don't help much in solving the eddy-current problem. To calculate the proximity-effect loss based on the classical definition, one has to know the field distribution and current distribution beforehand, which is almost impossible. To decompose loss into two parts that are easy to calculate and avoid analyzing the local proximity field in each conductor, we use a different definition of proximity-effect loss. We define proximity-effect loss in a winding as the loss due to the external field applied on a matrix of wire (the winding), and the corresponding definition of skin-effect loss is the total eddy-current loss minus that proximity-effect loss, which is equal to the loss in a conductor carrying time-varying net current and subjected to specified boundary conditions as shown in Fig. 2.

Fig. 2 shows in detail how the total current (including eddy current) in a winding is decomposed into skin-effect current in A and proximity-effect current in B by our definitions and also how the field on the winding is decomposed corresponding to the current decomposition. The fact that the currents in configuration A and B add up to current in C doesn't necessarily mean that the loss in A and the loss in B add up to loss in C. The total losses can be obtained by adding losses in A and B only if we can prove that orthogonality exists between skin effect and proximity effect in Fig. 2.

Reference [7] discussed conditions under which orthogonality is valid. A sufficient (but not necessary) condition for the sum of the loss in A and the loss in B to be identical to the total loss is that the conductor has an axis of symmetry in geometry and the current distribution in A has an odd
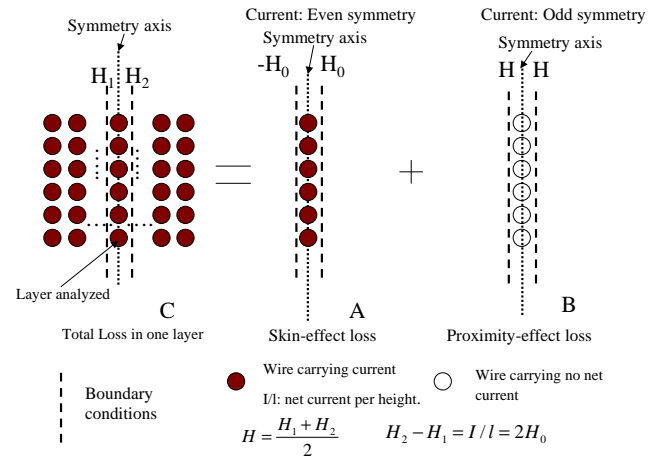
Fig. 2. Decomposition of total loss into skin-effect loss and proximity-effect loss in a winding.

symmetry about this axis while the current distribution in B has an even symmetry, or vice versa. It is straightforward that the configuration and current distributions in A and B in Fig. 2 satisfy these two conditions. Thus the total eddy-current loss in one conductor in C will be:

$$P_{total,ac} = P_{proximity-effect} + P_{skin-effect} \quad (1)$$

$$P_{proximity-effect} = \frac{\hat{G}H^2}{\sigma} \quad (2)$$

where $\hat{G}$ is the normalized unitless proximity-effect loss factor as in [12]: the proximity-effect loss per unit length in a conductor in a winding, normalized by the external field which the winding subjected to and by the conductivity, and H is the magnitude of external field or so-called 'proximity field' the winding is subjected to. From Fig. 2, we can see that the total field on the conductor can be decomposed into a uniform 'external field' component H plus H_0 or $-H_0$ caused by net current in the conductor, where H is the external field used to calculate proximity-effect loss and is the average of the fields on each side of the winding H_1 and H_2:

$$H = \frac{H_1 + H_2}{2} \quad (3)$$

Similar field decomposition method and orthogonality between skin effect and proximity effect also apply to foil-conductor windings. In the appendix, we show that the analysis of winding loss based on orthogonality leads to the same result as the analytical solution of field and loss in foil-conductor windings.

III. MODEL FOR CALCULATING PROXIMITY-EFFECT LOSSES IN A WINDING

In [12], we performed 4000 simulations for various winding geometries and various frequencies and then did curve fitting of $\hat{G}$ based on the simulation data. The results were given in the form of a function whose parameters are determined by

the winding geometry and can be looked up in a table. Our aim here is to create a similar function based on the same data from 2-D simulations but to avoid the unwieldy table needed in [12] by providing a function to calculate parameters directly from the geometry.

The new functional form of our model of the proximity-effect factor $\hat{G}$ is the weighted average of two different functions. One is called the modified Dowell function:

$$\hat{G}_1(X) = \frac{3\pi}{16} k^{-3} X \frac{\sinh(kX) - \sin(kX)}{\cosh(kX) + \cos(kX)} \quad (4)$$

where k is a function of wire spacings v/d and h/d and X is defined as:

$$X = \frac{d}{\delta} = d\sqrt{\pi \sigma \mu f} \quad (5)$$

where d is the diameter of the conductor, σ is the conductivity, μ is the permeability of the conductor material, and f is the frequency.

The other function is called the dual-slope function:

$$\hat{G}_2(X) = \frac{\pi}{32} \frac{X}{(X^{-3} + b^3)} \quad (6)$$

The dual-slope function was discussed in detail in [12].

The factors of $3\pi/16$ in (4) and $\pi/32$ in (6) ensure that both of them give the exact solution $\frac{\pi}{32}(\frac{d}{\delta})^4$ at very low frequencies $d/\delta \ll 1$, which is derived from the Bessel-function method's solution. At low frequencies, the Taylor expansion of $\frac{\sinh(kX)-\sin(kX)}{\cosh(kX)+\cos(kX)}$ is $\frac{1}{6}x^3k^3$. The k^3 factor in this expansion cancels the k^{-3} factor in (4), making $\hat{G}_1$ independent of k at low frequencies. Since k is the only parameter in (4) which is related to wire spacings, $\hat{G}_1$ is independent of the turn spacing, which makes physical sense, because at low frequencies, the field caused by eddy current in nearby conductors is very small and negligible. Compared to the function forms in [12], (4) and (6) are simpler and ensure the accuracy of the model in the low-frequency range when d/δ is much smaller than one.

As shown in [12], the (6) provides a better fit for some geometries, whereas (4) provides a better fit for other geometries. To allow fitting data with either shape, or any intermediate shape, we used a weighted average of the two functions (4) and (6), with weighting w:

$$\hat{G} = (1 - w)\hat{G}_1(X) + w\hat{G}_2(X) \quad (7)$$

By fitting (7) to the 100 sets of data (in each set of data d/δ sweeps from 0.6 to 60 with 40 samples evenly distributed on a log scale), we obtained 100 sets of w, k, and b values, defining curves which fit the data from 2-D FEA simulations much better than original Dowell model. Each set of values corresponds to a different v/d and h/d.

To use the results of curve-fitting and to avoid a large table as provided in [12], we studied different possible curve-fit functions that would give values of w, k and b based on the values of v/d and h/d.

In order to find $w(h/d, v/d)$, $k(h/d, v/d)$ and $b(h/d, v/d)$, first, we chose the appropriate models for the curve-fitting of

w, k and b versus h/d and v/d. By looking at plots of k and b, we found that the model

$$f(Y, s_1, s_2, q) = \frac{s_1 - s_2}{Y^{-1} + q^{-1}} + s_2 \quad (8)$$

would be able to describe accurately how b and w change with normalized interwire distance v/d and normalized interlayer distance h/d, where Y is the input—wire spacing v/d or h/d—whereas s_1, s_2 and q are parameters. It is a simplified form of the dual-slope function where s_1 and s_2 decide the two slopes, and q defines where the curve transitions between these two slopes.

Simulation data of proximity-effect loss factor $\hat{G}$ shows an overshoot at the transitions. This overshoot is exhibited by the modified Dowell function and does not exist in the dual-slope function. Thus, weighting w determines the extent of overshoot in (7). A model for the variation of w for various combinations of v/d and h/d can be constructed using curves of the form

$$w(Y) = c_1 \pm (u_1 - u_0 e^{-\frac{Y}{Y_0}})^2. \quad (9)$$

The shape of the $w(Y)$ curve is like a parabolic curve with a small input value Y and turns into a constant with large values of Y. Several such curves are combined with a weighting determined by h/d.

Second, we did curve-fitting for k, b and w. For example, to find the parameters for the model of $k(v/d, h/d)$, we first found 10 sets of s_1, s_2 and q for (8) for different values of h/d, and then chose the curve-fitting functions $s_1(h/d)$, $s_2(h/d)$ and $Tp(h/d)$. After the initial function forms and parameter values are found for k, b and w, we adjust all the parameters of $k(v/d, h/d)$, $b(v/d, h/d)$ and $w(v/d, h/d)$ simultaneously to make (7) fit the simulation data best. Finally, the functions for b, k and w can be given as:

$$b(v/d, h/d) = f\Big(v/d, \ f(h/d, s_{1b,1}, s_{2b,1}, q_{b,1}),$$

$$f(h/d, s_{1b,2}, s_{2b,2}, q_{b,2}), \ f(h/d, s_{1b,3}, s_{2b,3}, q_{b,3})\Big) \quad (10)$$

$$k(v/d, h/d) = f\Big(h/d, \ f(v/d, s_{1k,1}, s_{2k,1}, q_{k,1}),$$

$$f(v/d, s_{1k,2}, s_{2k,2}, q_{k,2}), \ f(v/d, s_{1k,3}, s_{2k,3}, q_{k,3})\Big) \quad (11)$$

$$w(v/d, h/d) = (h/d)w_1(v/d) + w_2(v/d)$$

$$w_1(v/d) = c_{11} - (u_{11} - u_{01} e^{-\frac{v/d}{Y_{01}}})^2$$

$$w_2(v/d) = c_{21} + (u_{21} - u_{02} e^{-\frac{v/d}{Y_{02}}})^2 \quad (12)$$

The parameters in (10), (11) and (12) are in Table. I.

The error of our model ((4), (6), (7), (8) and (10)–(12)) is within 4% in the range of frequency up to $d/\delta = 60$, v/d from 0.02 to 1.40, and h/d from 0.02 to 1.90, compared to FEA results both from the original 4000 simulations on which our curve-fitting is based, and also another 800 simulations we did for different interpolation values of h/d, v/d and f in the same range.

Fig. 3 compares maximum error for any geometry at a certain frequency given by each of three models: our model, the Dowell method, and the Bessel-function method. Errors are

TABLE I

PARAMETERS FOR b, k AND w TO BE USED IN (10), (11) AND (12)

		$s_{1b,j}$	$s_{2b,j}$	$q_{b,j}$
b	$j=1$	-0.0037	0.0432	-0.0661
	$j=2$	1.8167	0.0074	0.2195
	$j=3$	0.7053	0.8378	23.8755
		$s_{1k,j}$	$s_{2k,j}$	$q_{k,j}$
k	$j=1$	1.0261	0.8149	9.3918
	$j=2$	0.4732	0.8023	1.2225
	$j=3$	0.0930	0.2588	-0.0334
w	$c_{11}=0.0596$	$u_{11}=0.1558$	$u_{01}=0.3477$	$Y_{01}=1.0673$
	$c_{21}=0.0018$	$u_{21}=0.1912$	$u_{02}=0.2045$	$Y_{02}=1.3839$

relative to the simulation results which have less than 0.1% error. We can see that at frequencies where d/δ is larger than one, both the Bessel function method and the Dowell method can give very large error, from 60% to 120%, while our model only gives error less than 4%. At low frequencies, the Dowell method's error goes to 4.7%, while both the Bessel-function method and our model give error much smaller than that. At $d/\delta \ll 1$, the proximity-effect factors given by Bessel-function method and our model converge, and their error is below the simulation error of 0.1%.

A contour plot of maximum errors with various geometries is shown in Fig. 4. From Fig. 4, we can see that the largest error of our model—exceeding 3%—happens in geometries where the interlayer distance h is small and the interwire distance v is large, which is a rare situation in practical design—error there doesn't matter much. The largest error also happens when both v and h are very large. Based on 2-D simulation results shown in [12], proximity-effect factor increases with the increase of v/d and the decrease of h/d. To minimize the proximity-effect loss, generally we would like to have small v/d and large h/d. Fig. 4 shows that in the region of small v/d and large h/d, our model gives error smaller than 3%.

IV. FIELD CALCULATION FOR A TRANSFORMER

As discussed in Section II, the field magnitude H used for calculating proximity-effect loss is the average of the fields on each side of the conductor. In this section we will discuss how to calculate H for a simple transformer winding. However, the proximity-effect loss factor $\hat{G}$ is independent of the overall field and can be used broadly in various field shapes.

In the pth layer of a simple layer-wound transformer winding of m layers, the magnitude of external field is:

$$H = \frac{(2p-1)}{2}\frac{NmI}{b_w} \qquad (13)$$

where b_w is the breath of winding window, N is the total number of turns, and I is the peak current carried by each turn.

For the convenience of using (13) in (1), we can obtain the average of square of the field in m layers:

$$\overline{H^2} = \frac{1}{3}\frac{(NI)^2}{b_w{}^2}\left(1 - \frac{1}{4m^2}\right) \qquad (14)$$

Assuming that the field varies linearly over the winding layer thickness and that the number of layers is very large,
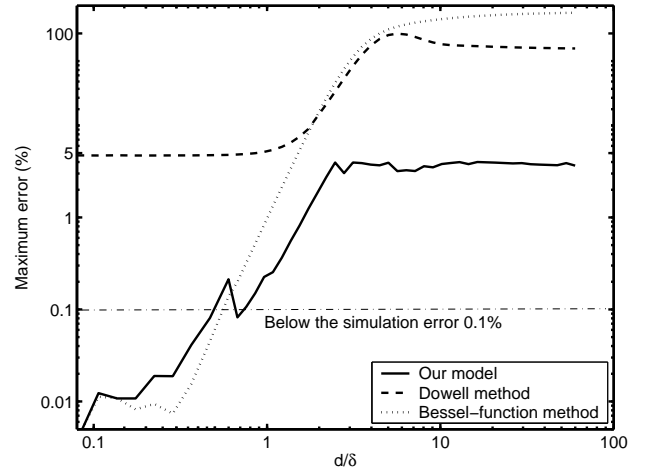
Fig. 3. This plot compares the maximum error for any geometry at a certain frequency given by each of the three models: our model, the Dowell method, and the Bessel-function method. At low frequencies, the Dowell method's error goes to 4.7%, while both the Bessel-function method give error much smaller than that. At $d/\delta \ll 1$, the proximity-effect factors given by Bessel-function method and our model converge, and their error is below the simulation error of 0.1%. At higher frequencies, our model always gives a more accurate prediction than the Dowell method (up to 60% error) and the Bessel-function method (up to 120% error).
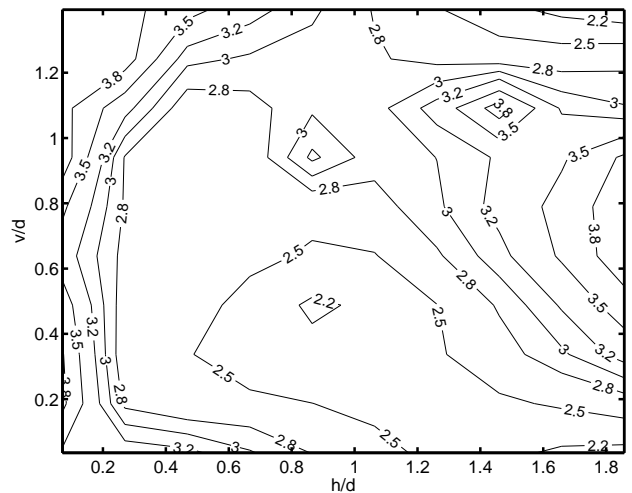
Fig. 4. Maximum error (%) of our model ((7)-(12)) relative to simulation results over the frequency range corresponding to d/δ from 0.6 to 60 is within 4%. Generally our model gives a smaller error (within 3%) at smaller interwire distance v, which is the geometry most frequently used in practice.

the most generally used average field for a multilayer winding is [15]:

$$\overline{H^2} = \frac{1}{3}\frac{(NI)^2}{b_w^2} \qquad (15)$$

Although (14) is a better formula to use especially for a one or two layer winding, when the number of layers is large, the error of (15) compared to (14) is very small. For example, the error is less than 3% at $m=3$.

V. DISCUSSION OF SKIN-EFFECT LOSSES OF A CONDUCTOR IN A WINDING

The loss increase at high frequencies caused by skin effect for a single isolated round conductor can be expressed in the

form of the ratio of AC resistance and DC resistance [6]:

$$\frac{R_{ac,skin}}{R_{dc}} = \frac{\gamma}{2} \frac{ber\gamma bei'\gamma - bei\gamma\gamma ber'\gamma}{ber'^2\gamma + bei'^2\gamma} - 1 \quad (16)$$

where γ is:

$$\gamma = \frac{1}{\sqrt{2}}\frac{d}{\delta} = \frac{1}{\sqrt{2}}X \quad (17)$$

Equation (16) is for a conductor carrying a specified current which is not subjected to any external field. But according to our definition of skin-effect loss, the skin-effect loss of conductors in a winding will be larger than that in (16) because the current distribution will be affected by other conductors, even in a layer which is not subjected to any external 'proximity' field.

We performed 2-D FEA simulation for a configuration as shown in Fig. 5 to find out the scope of error caused by using (16) to calculate skin-effect loss in our definition. Fig. 5 is an equivalent setup for A in Fig. 2. At $d/\delta = 8$, the difference between the loss prediction of (16) and the simulation result is about 20% of the skin-effect loss and 11% of the skin-effect loss plus resistive loss. However, this difference is only about 1% of the total loss which also includes the proximity-effect loss in a one-layer winding. When the number of layers increases, proximity-effect loss becomes more significant and dominates the total loss, the error in calculating skin-effect loss is negligible in the total loss.

In a one-layer winding, the percentage of error caused by using approximate skin-effect loss calculation is given in Fig. 6. In a multi-layer winding, this error will continue to decrease as the number of layers increases. Thus we can use (16) for calculating the skin-effect loss in our model.
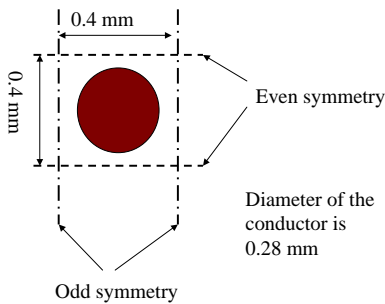
Fig. 5.   Configuration of FEA simulation for skin-effect loss

VI. EXPERIMENTAL RESULTS

To validate the accuracy of our new model, we did loss measurements on three different types of windings. All of the three windings are on pot cores (42 mm × 29 mm) of MnZn ferrite (Philips 3F3). All of the three windings contain three layers of primary winding and three layers of secondary winding. The two windings are wound in opposite directions and are connected in series opposition to achieve small inductance in the winding so that accurate measurement of small winding resistance is easier. We used an impedance
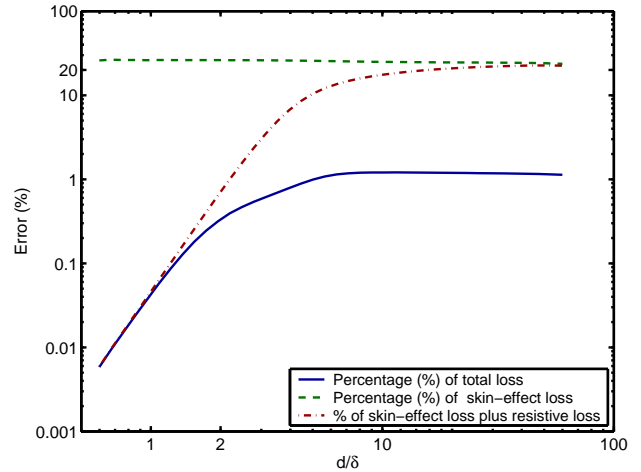
Fig. 6.   Inaccuracy produced by using approximate formula (16) is below 1% of the total winding loss. Though using (16) to calculate the skin-effect loss (by our definition) can produce error as large as 20%, this error is negligible in the total eddy-current loss, in which skin-effect loss is always a small part over the frequency range. The plot is for a one-layer winding with $v/d = 0.4286$ and $h/d = 0.4286$. In a multilayer winding, inaccuracy in calculating skin-effect loss will be even more insignificant compared to the total loss, because proximity-effect loss dominates.
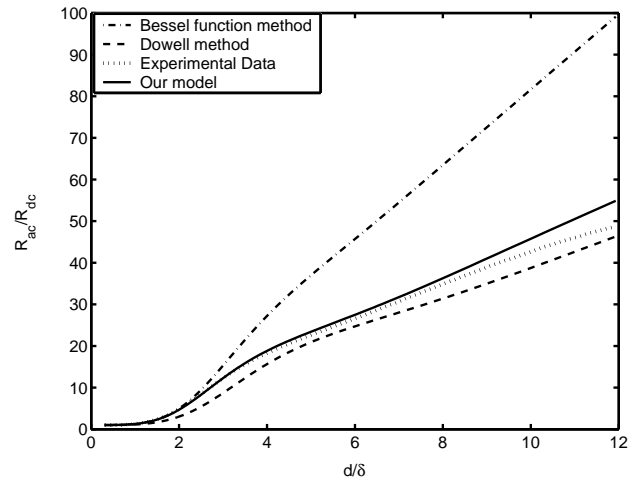
Fig. 7.   Comparison of experimental data for winding type A to the results given by our new model

analyzer to measure the AC resistance over the frequency range of 1 kHz to 2.5 MHz. Also, the error caused by the parasitic capacitance was compensated using the circuit model in [16]. Specifications of the three winding types are in Table II.

In Fig. 7, Fig. 8 and Fig. 9, we can see that our model fits the experimental data better than either the Dowell model and the Bessel-function model.

Winding type A and winding type C have the same interwire distance v and same wire diameter, while winding C has a larger interlayer distance h than winding type A. Winding A will have larger winding loss according to our model's prediction. Though the difference in loss between experimental data in Fig. 7 and 9 is not obvious, a closer examination of the experimental data revealed that at d/δ around 3 the

TABLE II

SPECIFICATIONS OF THE WINDINGS MEASURED

Winding type	Wire	Insulation on wire	Insulation between layers	Actual average v/d	Actual average h/d
A	22 AWG magnet wire	single build	one layer of tape	0.28	0.29
B	22 AWG solid wire	0.25 mm teflon	—	1.43	1.43
C	22 AWG magnet wire	single build	5 layers of polypropylene tape	0.29	1.50
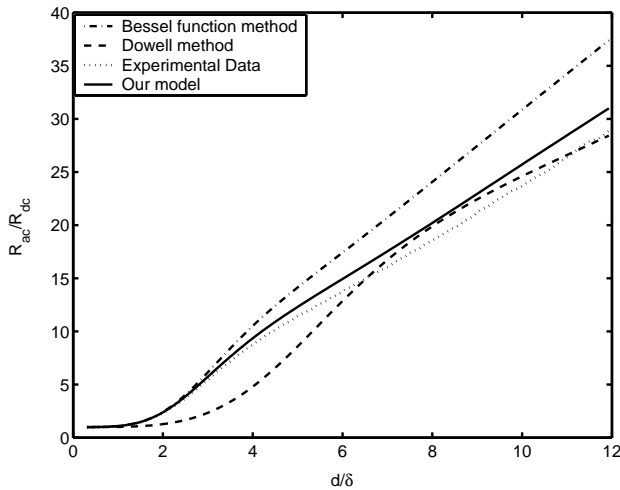
Fig. 8.   Comparison of experimental data for winding type B to the results given by our new model
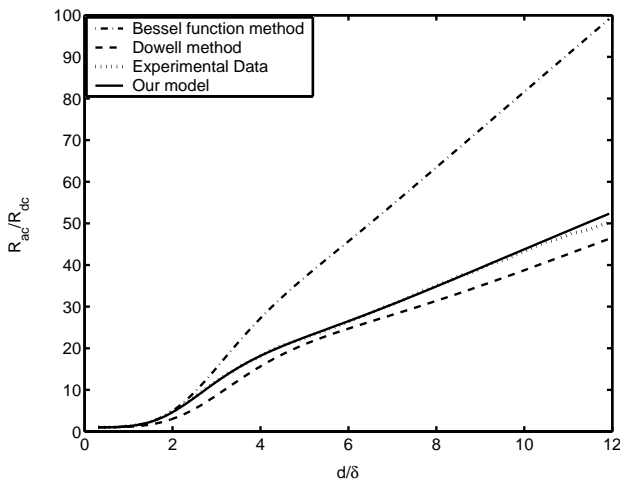
Fig. 9.   Comparison of experimental data for winding type C to the results given by our new model

loss in type C is 1% larger than the loss in type A, which matches the prediction of our model. At higher frequencies, our experimental data on winding type A and C doesn't show the same loss difference. This may be due to the limitation of our compensation of parasitic capacitances.

Loss in winding type B is smaller than that of winding type A or that of winding type C. This is because there are fewer turns per layer in winding type B and smaller H. To minimize the proximity-effect loss for the same number of turns, winding type C, with minimum interwire distance and

large interlayer distance, will be the best.

VII. CONCLUSION

In this paper, based on 2-D FEA simulation data, we present a complete model for calculating the eddy-current winding losses in a winding of round conductors. Compared to other methods, our method of calculating winding loss has the following advantages: First, our method's results are based on FEA simulations on a 2-D model of the winding, which are inherently more accurate than the previously used approximate models such as Dowell's 1-D model and the Bessel-function model, which neglects the interactions between conductors. Second, our loss model is able to describe the behavior of a winding with various geometry parameters over a wide frequency range, and our method separates overall field analysis from the analysis of local eddy currents thus the result can be extended to any field shape. Third, our model is presented as a closed-form function, such that designers can use it directly to calculate loss and thus avoid the pain of FEA simulations.

ACKNOWLEDGMENT

REFERENCES

[1] Glenn R. Skutt Thomas G.Wilson Audrey M. Urling, Van A. Niemela, "Characterizing high-frequency effects in transformer windings–a guide to several significant articles", *Journal of Circuits, Systems, and Computers*, vol. 5, Dec. 1996.

[2] P.L. Dowell, "Effects of eddy currents in transformer windings", *Proceedings of the IEE*, vol. 113, no. 8, pp. 1387–1394, Aug. 1966.

[3] P.S.Venkatraman, "Winding eddy current losses in switch mode power transformers due to rectangular wave currents", *Proceedings of Powercon 11,Power Concepts Inc.*, pp. 1–11, 1984.

[4] M.P. Perry, "Multiple layer series connected winding design for minimum losses", *IEEE Transactions on Power Apparatus and Systems*, vol. PAS-98, pp. 116–123, Jan./Feb. 1979.

[5] E.Bennet and S.C. Larson, "Effective resistance of alternating currents", *American Institute of Electrical Engineers*, vol. 59, pp. 1010–1017, 1940.

[6] Richard L. Stoll, *The analysis of eddy currents*, Clarendon Press. Oxford, 1974.

[7] J. A. Ferreira, "Improved analytical modeling of conductive losses in magnetic components", *IEEE Transactions on Power Electronics*, vol. 9, no. 1, pp. 127–31, Jan. 1994.

[8] Massimo Bartoli, Nicola Noferi, Alberto Reatti, and Marian K. Kazimierczuk, "Modeling litz-wire winding losses in high-frequency power inductors", in *27th Annual IEEE Power Electronics Specialists Conference*, June 1996, vol. 2, pp. 1690–1696.

[9] William R. Smythe, *Static and Dynamic Electricity*, McGraw-Hill, 1968, page 411.

[10] J. A. Ferreira, "Analytical computation of ac resistance of round and rectangular litz wire windings", *IEE Proceedings-B Electric Power Applications*, vol. 139, no. 1, pp. 21–25, Jan. 1992.

[11] J. A. Ferreira, *Electromagnetic Modelling of Power Electronic Converters*, Kluwer Academic Publishers, 1989.

[12] Xi Nan and Charles R. Sullivan, "An improved calculation of proximity-effect loss in high frequency windings of round conductors", in *PESC03*, 2003, vol. 2, pp. 853–860.

[13] Charles R. Sullivan, "Computationally efficient winding loss calculation with multiple windings, arbitrary waveforms, and two- or three-dimensional field geometry", *IEEE Transactions on Power Electronics*, vol. 16, no. 1, pp. 142–150, Jan. 2001.

[14] Alexander D. Podoltsev, "Analysis of effective resistance and eddy-current losses in multiturn winding of high-frequency magnetic components", *IEEE Transactions on Magnetics*, vol. 39, no. 1, pp. 539–548, Jan. 2003.

[15] E. C. Snelling, *Soft Ferrites, Properties and Applications*, Butterworths, second edition, 1988.

[16] Charles R. Sullivan, "Optimal choice for number of strands in a litz-wire transformer winding", *IEEE Transactions on Power Electronics*, vol. 14, no. 2, pp. 283–291, 1999.

[17] J. H. Spreen, "Electrical terminal representation of conductor loss in transformers", *IEEE Transactions on Power Electronics*, vol. 5, no. 4, pp. 424–9, 1990.

APPENDIX

The decomposition of orthogonal skin effect and proximity effect in Fig. 2 works for any conductor or group of conductors which has a symmetric shape. We can use the foil conductor as an example to explain how the orthogonality works and show that the average of the fields on each side of the winding is the right H to use for (2). The loss per unit length in a foil conductor is given in [17]:

$$P = \frac{1}{2}\frac{b\rho}{\delta}[(H_1 - H_2)^2 F(h/\delta) + 2H_1 H_2 G(h/\delta)] \quad (18)$$

where h is the thickness of the conductor, b is the width of the conductor, ρ is the resistivity of the conductor, H_1 and H_2 are the field magnitudes on each side of the foil, and F and G are functions of the skin depth δ:

$$F(x) = \frac{sinh(2x) + sin(2x)}{cosh(2x) - cos(2x)} \quad (19)$$

$$G(x) = \frac{sinh(x) - sin(x)}{cosh(x) + cos(x)} \quad (20)$$

The loss per unit length in a foil conductor which is subjected to an external field of peak value H is:

$$P_{proximity} = \frac{b\rho}{\delta}H^2 G(h/\delta) \quad (21)$$

The skin-effect loss in a foil conductor in a winding window will be:

$$H_1 = -H_2 = \frac{I}{2b}; \qquad P_{skin} = \frac{\rho}{2\delta}\frac{I^2}{b}(F(h/\delta) - \frac{1}{2}G(h/\delta)) \quad (22)$$

Then if we consider a one-layer winding, we know that for that layer:

$$H_1 = 0; \qquad H_2 = \frac{I}{b} \quad (23)$$

For the proximity-effect loss, if we use field H as average of H_1 and H_2:

$$P_{proximity} = \frac{\rho}{\delta}\frac{I^2}{4b}G(h/\delta) \quad (24)$$

Equation (22) gives the expression for skin-effect loss. Either by plugging (23) into (18) or by add (22) and (24), we get an identical total loss expression for a one-layer winding:

$$P = \frac{\rho}{2\delta}\frac{I^2}{b}F(h/\delta) \quad (25)$$

This shows that the decomposition Fig. 2 works and that the average of the values of H on each side of a winding layer is the correct value to use in (2) to calculate loss.

For the p_{th} layer in a multilayer foil winding,

$$H_1 = \frac{(p-1)I}{b} \quad (26)$$

$$H_2 = \frac{pI}{b} \quad (27)$$

$$H = \frac{(2p-1)I}{2b} \quad (28)$$

$$P_{proximity} = \frac{b\rho}{\delta}\frac{(2p-1)^2 I^2}{4b^2}G(h/\delta) \quad (29)$$

$$
\begin{aligned}
P_{proximity} &+ P_{skin} \\
&= \frac{b\rho}{\delta}\frac{(2p-1)^2 I^2}{4b^2}G(h/\delta) + \frac{\rho}{2\delta}\frac{I^2}{b}(F(h/\delta) - \frac{1}{2}G(h/\delta)) \\
&= \frac{\rho}{2\delta}\frac{I^2}{b}[F(h/\delta) + 2p(p-1)G(h/\delta)] \\
&= \frac{1}{2}\frac{b\rho}{\delta}[(H_1 - H_2)^2 F(h/\delta) + 2H_1 H_2 G(h/\delta)] \quad (30)
\end{aligned}
$$

The above calculations again prove the validity of the decomposition in Fig. 2.